Available online at www.sciencedirect.com

ScienceDirect

journal homepage: www.elsevier.com/locate/issn/15375110

Research Paper

Prediction mapping of physicochemical properties in mango by hyperspectral imaging

Parika Rungpichayapichet [a], Marcus Nagle [a,*], Pasinee Yuwanbun [b], Pramote Khuwijitjaru [b], Busarakorn Mahayothee [b], Joachim Müller [a]

[a] Institute of Agricultural Engineering, Tropics and Subtropics Group, Universität Hohenheim, Garbenstrasse 9, Stuttgart, 70599, Germany

[b] Department of Food Technology, Faculty of Engineering and Industrial Technology, Silpakorn University, Nakhon Pathom, 73000, Thailand

ARTICLE INFO

Article history:
Received 16 February 2016
Received in revised form
21 March 2017
Accepted 15 April 2017

Keywords:
Mangifera indica
Fruit quality
Hyperspectral imaging
Chemometrics
Spectral mapping
vis-NIR spectroscopy

Hyperspectral imaging (HSI) techniques using a newly-developed frame camera were applied to determine internal properties of mango fruits including firmness, total soluble solids (TSS) and titratable acidity (TA). Prediction models were developed using spectral data from relative surface reflectance of 160 fruits in the visible and near infrared (vis/NIR) region of 450–998 nm analysed by PLS regression. For data reduction, MLR analysis showed 16 significant factors for firmness, 17 for TA, and 20 for TSS. The results of MLR did not substantially affect the prediction performance as compared to PLS. An original approach with combined chemometric and HSI data analyses was applied using R programming. Significant correlations were found between HSI data and firmness (R^2 = 0.81 and RMSE = 2.83 N) followed by TA (R^2 = 0.81 and RMSE = 0.24%) and TSS (R^2 = 0.5 and RMSE = 2.0%). Prediction maps of physicochemical qualities were achieved by applying the prediction models to each pixel of HSI to visualise their spatial distribution. The variation of firmness, TSS, and TA within the fruit indicated fruit ripening started from shoulder toward to tip part. From these results, HSI can be used as a non-destructive technique for determining the quality of fruits which could potentially enhance grading capabilities in the industrial handling and processing of mango.

1. Introduction

Mango quality plays an important role on market price and consumer satisfaction. Superior quality induces a customer's willingness to pay premium prices for a product. Overall, physical appearances such as colour and firmness are considered the primary criteria customers use to evaluate fruit quality (Delwiche, Mekwatanakarn, & Wand, 2008). Sivakumar, Jiang, and Yahia (2011) have meanwhile reported that consumer preference and order decisions are more related to fruit taste. However, in commercial operations, heterogeneous fruit quality is encountered due to the variation in degree of ripeness of harvested fruits, which causes non-uniform ripening behaviour and requires different

* *Corresponding author*. Fax: +49 (0)711 459 23298.
E-mail address: info440e@uni-hohenheim.de (M. Nagle).
http://dx.doi.org/10.1016/j.biosystemseng.2017.04.006

postharvest handling (Kienzle et al., 2012). This problem leads to reduced shelf-life and postharvest losses during handling and transport. Therefore, inspection and controlling quality of mango at packing is an imperative process in the mango industry to assure that only superior fruits are distributed to high-value markets.

The potential of non-destructive techniques as tools for sorting and grading have been demonstrated in numerous studies. Near infrared spectroscopy (NIRS) is widely implemented to identify the quality of many fruits, including mango. Studies have shown the potential of NIRS to determine the physicochemical properties of mango such as firmness, total soluble solids content (TSS), titratable acidity (TA) and bioactive compounds (Jha, Narsaiah et al., 2010; Nagle, Mahayothee, Rungpichayapichet, Janjai, & Müller, 2010; Rungpichayapichet, Mahayothee, Khuwijitjaru, Nagle, & Müller, 2015; Rungpichayapichet, Mahayothee, Nagle, Khuwijitjaru, & Müller, 2016; Subedi & Walsh, 2011; Theanjumpol, Self, Rittiton, Pankasemsuk, & Sardsud, 2014; Valente, Leardi, Self, Luciano, & Pain, 2009; Watanawan, Wasusri, Srilaong, Wongs-Aree, & Kanlayanarat, 2014). More recently, hyperspectral imaging (HSI) is being regarded as an effective non-destructive method to determine the quality of agricultural products. The advantages of HSI over NIRS are the simultaneous procurement of spatial and spectral information from the sample and the flexibility of area selection for spectral extraction after data acquisition (Schmilovitch et al., 2014; Zhang, Liu, He, & Gong, 2013). Overall, HSI can provide information on the spatial distribution of physicochemical parameters, enhancing the perception of quality changes within samples (ElMasry, Sun, & Allen, 2013). The ability of HSI to evaluate the quality of fruits was recently reviewed by Magwaza and Opara (2015). For mango, HSI has been applied to detect fruit fly infestation (Haff et al., 2013; Saranwong et al., 2011), mechanical damage (Vélez Rivera et al., 2014), moisture distribution in dried mango slices (Pu & Sun, 2015) and postharvest qualities including colour, firmness and TSS (Makino et al., 2013; Sivakumar, 2006). However, little documentation currently exists describing the variability of physicochemical qualities within mango fruits and studies applying HSI to monitor these spatial quality changes are lacking. Issues also remain with software for HSI analysis, especially with respect to real-time application (ElMasry & Nakauchi, 2016) and high computational requirements for HSI data. Therefore, this study aims to demonstrate the feasibility of HSI as a tool to observe the spatial changes of quality of mango during ripening by (i) testing hyperspectral frame camera technology for rapid image acquisition, (ii) developing reduced-factor HSI prediction models in freely-available, programmable software to quantitatively determine physicochemical qualities of mango, and (iii) establishing prediction maps showing the distribution pattern of quality parameters within fruits for potential grading applications.

2. Materials and methods

2.1. Materials

A total of 160 mango fruits (cv. Nam Dokmai, subcv. Si Thong) from two production areas (Phitsanulok and Phetchabun provinces, Thailand) were obtained at commercial export maturity, corresponding to 120 days after full bloom. Eighty fruits from each area were harvested during the peak season in April 2013. Mature fruits were preselected in the field for fruit mass about 310 g and density greater than 1000 kg m^{-3}. Fruits then were transported to Nakhon Pathom province within one day, where the experiments were carried out. Fruits free from visual defects were washed, air-dried, and stored in baskets covered with paper at ambient temperature (32.1 ± 0.6 °C and 73.0 ± 7.9% relative humidity) for up to 8 days of ripening. Ten fruits were randomly selected each day and subjected to HSI analysis and quality reference measurements.

2.2. Reference analyses of quality attributes

Fruits were cut along the sagittal plane from the proximal to distal end into two slabs on either side of the endocarp. Slabs were divided into three positions, i.e. shoulder, cheek, and tip parts (Fig. 1a). Firmness was determined only at the cheek position according to Jha, Kingsly, and Chopra (2006). A puncture test was performed with a needle probe (2 mm diameter) on the peeled mesocarp at a speed of 0.5 mm s^{-1} and a compression depth of 10 mm using a texture analyser (TA-xT2i, Stable Micro Systems, Godalming, UK). Maximum force (N) was used to describe the firmness. For chemical analyses, each mesocarp section was homogenised separately (Ultra-Turrax T25 basic, IKA Labortechnik, Germany). Five grams of the homogenate was squeezed through filter cloth and used to determine TSS by a digital refractometer (PAL-1, Atago, Tokyo, Japan). TA was measured by alkaline titration of 100 mL dilution prepared from 5 g of homogenate with 0.1 N NaOH until a pH of 8.1 and expressed as mass percentage (%) of citric acid (AOAC, 1999). Determinations of TSS and TA were done in duplicate.

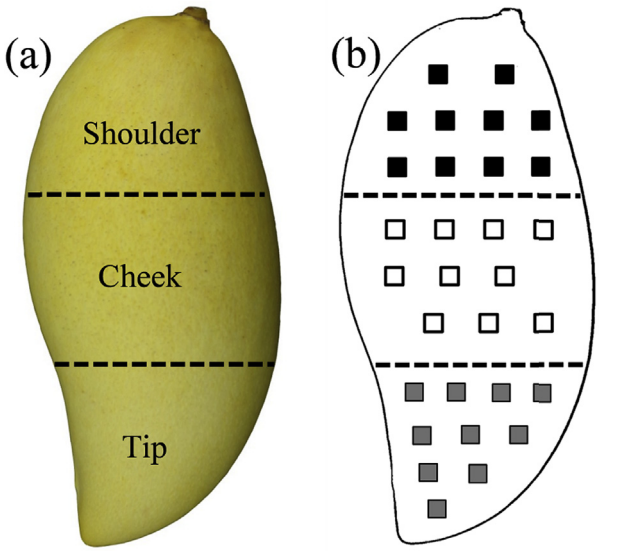

Fig. 1 – Fruit positions for (a) reference quality analyses sampling and (b) region of interest (ROI) selection for hyperspectral measurements; ROIs are not to scale.

2.3. Hyperspectral system and image acquisition

A HSI measurement system was setup for spectral data acquisition in this study (Fig. 2), which was similar to the equipment and methods used by Jung, Vohland, and Thiele-Bruhn (2015). The system consisted of (i) a sample holder (ii) a 50 W tungsten halogen lamp (Pro Lamp, ASD Inc. CO, USA) and (iii) a hyperspectral frame camera UHD 285 (Cubert GmbH, Ulm, Germany), which has been developed for the advantage of real-time data acquisition (Hagen, Kester, Gao, & Tkaczyk, 2012). The distance between the camera and the sample was fixed at 700 mm. The hyperspectral imaging system was controlled by a PC with the Cubert GUI (Cubert GmbH, Ulm, Germany). Prior to image acquisition, the light source was switched on for 15 min to stabilise illumination. In addition, two light-diffusers (150 × 250 mm) were placed nearby the sample holder to provide uniform light distribution. Images were acquired at a spatial dimension of 910 × 900 pixels, with a respective pixel size of 0.32 × 0.32 mm representing a pixel area of 0.10 mm^2. The integration time required for capturing the complete hyperspectral image was 10 ms. Spectral data included 138 bands covering the spectral range 450–998 nm in 4 nm increments with a spectral resolution of 8 nm. Dark reference was measured with the shutter closed while covering of the camera lens with black paperboard. A professional light reflector disc made from Teflon-coated nylon fabric was used as white reference. Image correction was done automatically by Cubert software according to Eq. (1).

$$\%RI = \frac{IS(x,y)|ID(x,y)}{IR(x,y) - ID(x,y)} \times 100 \quad (1)$$

where *RI* is the relative reflectance at pixel location (x, y) in percentage, *IS* is the sample image value, *ID* is the dark frame image value and *IR* is the white reference image value (Leiva-Valenzuela, Lu, & Aguilera, 2014).

2.4. Data analysis

2.4.1. Spectral analysis

The spectral information was extracted from hyperspectral image file using HyperSpec interface (Beleites & Sergo, 2012) in the R environment (version 3.1.0, R Core Team, 2014). Ten region of interest (ROI) areas of 10 × 10 pixels were defined in each of the fruit segments (Fig. 1b). The reflectance spectrum of each ROI was averaged from the corresponding 100 pixels. The HSI data from the three fruit sections (shoulder, cheek, and tip), representing the respective reference measurements, were used to develop the calibration models. In addition, RGB and monochromatic images at frequencies corresponding to chlorophyll (680 nm) and sucrose (913 nm) were generated from the Cubert software provided with the camera. Images were converted to greyscale in ImageJ software (Rasband, 2014) where the fruit area was automatically identified and subsequent light intensity (I_L) of the fruit surface, as a mean of pixel values ranging from 0 (black) to 255 (white) was calculated by the software.

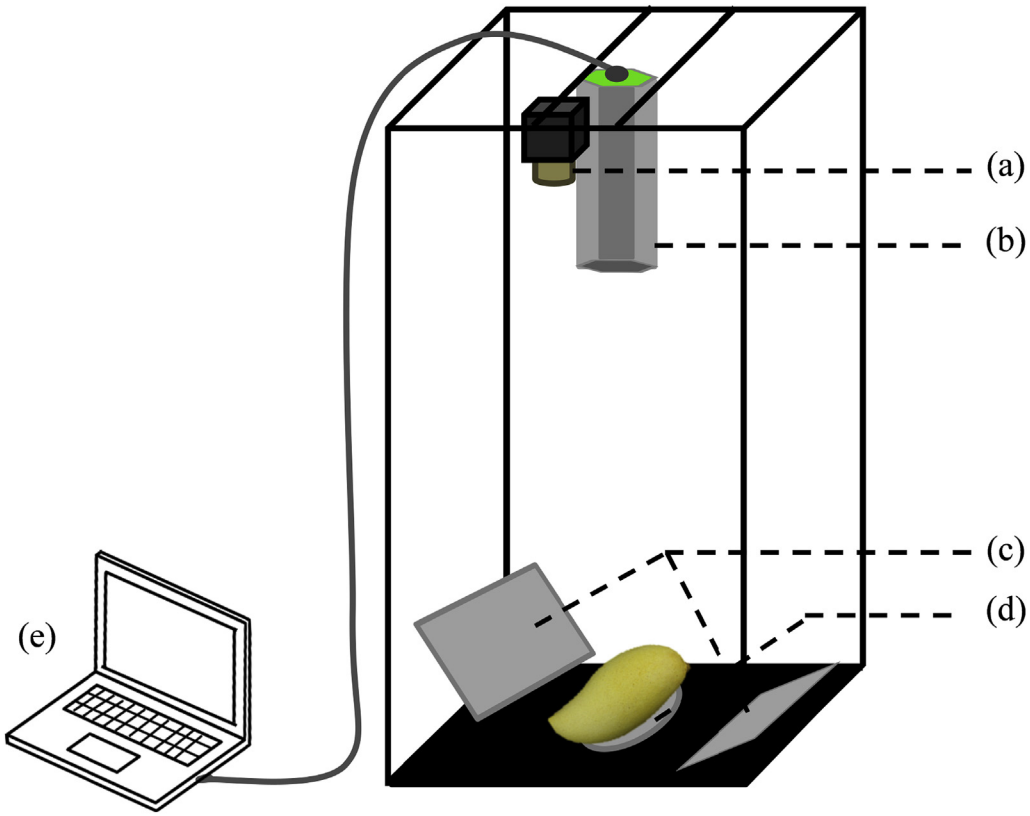

Fig. 2 – Hyperspectral imaging system: (a) tungsten halogen lamp, (b) hyperspectral frame camera with CCD detector, (c) mirrors, (d) sample holder and (e) computer with data acquisition software.

2.4.2. Regression model development

A total of total of 4800 reflectance spectra were obtained from 160 fruits (10 spectra from each section resulting in 30 spectra per fruit). To establish calibration and validation sets, fruit samples were sorted according to their physicochemical values. The two highest and two lowest values were assigned to the calibration set. After that, two-thirds of the samples were fixed as calibration data and one-third of the samples were defined as validation data in a 2:1 leave-one-out procedure. Thus, calibration data was established from 3240 reflectance spectra (67.5% of the measured spectra) using full-cross validation and the remaining 1560 reflectance spectra (32.5%) were set as external validation samples.

Different mathematical pre-processing of the spectra were performed during building of prediction models to improve the performance, including Savitzky–Golay smoothing (SG), Savitzky–Golay second derivative (SG″) using 15 points with second order polynomial regression (Savitzky & Golay, 1964), standard normal variate (SNV) transformation and multiplicative scatter correction (MSC) using the 'prospectr' package for R (Stevens & Ramirez-Lopez, 2013). Models were formulated to relative reflectance spectra and reference values for each fruit part by applying partial least squares (PLS) regression using the full cross-validation method (Mevik & Wehrens, 2007). Multifactorial analysis (backward-elimination-stepwise method) was used for selecting significant wavelengths. Candidate variables were chosen from wavelengths which were found to be related with quality by PLS regression coefficient plots. Multiple linear regression (MLR) was used to develop the reduced-factor models. Performance of the prediction models was evaluated using coefficient of determination (R^2), root mean square error (RMSE) and bias. The model fit was assessed based on high R^2, low RMSE and low bias. These parameters are defined as follows, according to Esbensen (2004, chap. 9):

$$RMSE = \sqrt{\frac{1}{n}\sum_{i=1}^{n}\left(\hat{y}_i - y_i\right)^2} \quad (2)$$

$$bias = \frac{1}{n}\sum_{i=1}^{n}\left(\hat{y}_i - y_i\right) \quad (3)$$

where $\hat{y}_i$ is the predicted values calculated by the calibration equation; y_i is the measured values obtained from the reference analysis; n is the number of samples used in the calibration ($RMSE_{cal}$) and validation ($RMSE_{val}$), respectively. The number of PLS components was defined based on combination of high R^2 together with low $RMSE_{cal}$ and $RMSE_{val}$ representing goodness-of-fit for the prediction models.

2.4.3. Hyperspectral classification of physicochemical properties

Prediction maps of firmness, TA and TSS were generated using graphics functions programmed in R language by applying the PLS prediction model to each pixel with its own corresponding spectrum. The prediction results of each pixel have been displayed and plotted according to the constituent of the sample based on their spectral signature to provide the distribution gradient in the sample (ElMasry et al., 2013). Prediction images of mango quality during ripening were established by applying the best prediction model to all pixels in segmented HSI images (background removed). Spatial distributions of physicochemical attributes were illustrated by colour gradients which were used to depict respective values in the fruit samples. Prediction maps for the three predicted parameters required 9.5 s to generate using the programmed functions. Discriminant analysis (DA) was applied to HSI spectral data using SPSS software (ver. 16.0, SPSS, Inc., Chicago, IL) to classify fruits according to ripeness. Mean spectra from three positions were subjected to DA and the classification model was validated using cross-validation method.

2.4.4. Statistical analyses

Statistical analyses were performed using SAS program (version 9.3, SAS Inst., New Jersey, USA). Data was assessed for correlations between the individual quality parameters. Relationships were evaluated using Pearson correlation coefficient and level of significance (p value). General linear model program (GLM) and least significant difference (LSD) were applied to determine significant differences between chemical compositions for each fruit position using ripening day as blocks. The results were assessed at the significance level $p \leq 0.05$. The difference between laboratory reference methods (measured) and HSI-predicted quality parameters were analysed by conducting paired t-tests.

3. Results

3.1. Physicochemical changes during ripening

Physicochemical changes of mango during ripening (also respective to fruit position) are shown in Fig. 3. Firmness was found to clearly decrease in the initial phase of ripening and decline more gradually in the final phase. Significant differences of firmness were found from the first to fifth day of ripening, decreasing from 25.04 to 8.45 N and then further declining to 6.32 N (Fig. 3a). Ketsa, Chidtragool, Klein, and Lurie (1998) reported that softening of mango pulp takes place by breakdown of the structurally-bound pectin in the cell wall into water-soluble pectin by β-galactosidase and polygalacturonase. In addition, firmness decline can be augmented by starch deterioration during ripening (Yashoda, Prabha, & Tharanathan, 2006). TA sharply declined in the first phase of ripening and thereafter reduced slightly over the end phase (Fig. 3a and d). Significant reductions in TA (85%) were found over the first four days of ripening, from 1.65 to 0.25% (Fig. 3b). Vélez Rivera et al. (2014) reported that acid degradation of mango is mainly caused by metabolism of citric acid. Figure 3c illustrates the increase of TSS during ripening. Significant differences were found on first three days of ripening, when TSS rose sharply from 13.5 to 18.8%, then continued to moderately increase to a maximum of 19.5% on the sixth day of ripening (Fig. 3c). Increasing sweetness during ripening is a result of starch hydrolysis by amylase, whereas slight decreases in the final phase may be due to conversion by respiration or fermentation during senescence (Jha et al., 2006; Medlicott & Thompson, 1985; Palafox-Carlos et al., 2012). With respect to fruit position, variations of TA and TSS in individual fruits were clearly observed (Fig. 3d and e). Significant differences of TA at different fruit parts were found during the

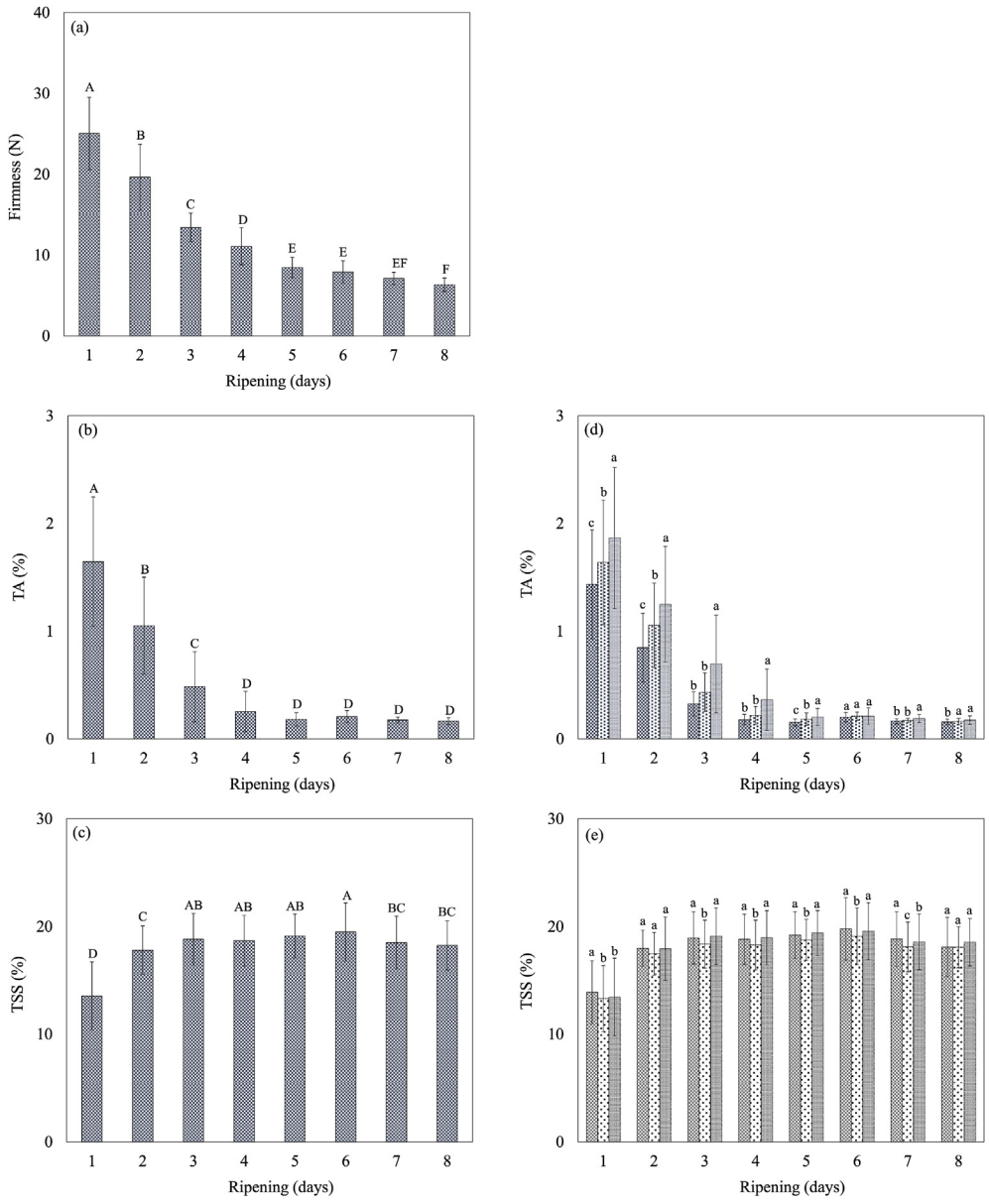

Fig. 3 – Mean values of (a) firmness, (b) TA, and (c) TSS as well as differences in (d) TA and (e) TSS within fruit samples during ripening.

initial phase of ripening (Fig. 3d). The highest acidity was observed at the tip part, while the shoulder part was significantly lower in concentration of organic acids. Shoulder parts had the highest TSS contents, but did not significantly differ from the tip parts. The results indicated that overall ripening process of mango cv 'Nam Dokmai' progressed from the shoulder toward the tip part. Results also showed that all three quality parameters were significantly correlated with one another at $p < 0.001$. The clearest relationship was TA:F with $r = 0.93$, while correlations with TSS were weaker ($r = -0.66$ for TSS:TA and $r = -0.62$ for TSS:F).

3.2. *Reflectance imaging*

RGB images, monochromatic images at 680 and 913 nm and the average original reflectance spectra of mango are shown in Fig. 4. A characteristic of the Nom Dokmai cultivar is the pale yellow (in the web version) peel colour at the unripe stage that changes to intense yellow during ripening, which is evident in the RGB images. The images at 680 and 913 nm are shown for monitoring the changes of chlorophyll and sugar content during ripening, respectively, since these wavelengths are responsive to the corresponding compounds (ElMasry, Wang, ElSayed, & Ngadi, 2007; McGlone & Kawano, 1998). Differences between the images at 680 and 913 nm were not clearly seen at the same ripening day, while noticeable changes were found between ripening days. A relative reflectance was observed in fruits at 680 nm on the first day of ripening. Mango at the unripe stage showed higher reflectance as seen by the brighter image as compared to ripened samples. For example, I_L at 680 nm changed from 121 to 101, whereas I_L at 913 nm decreased from 111 to 80 during ripening. A higher relative reflectance

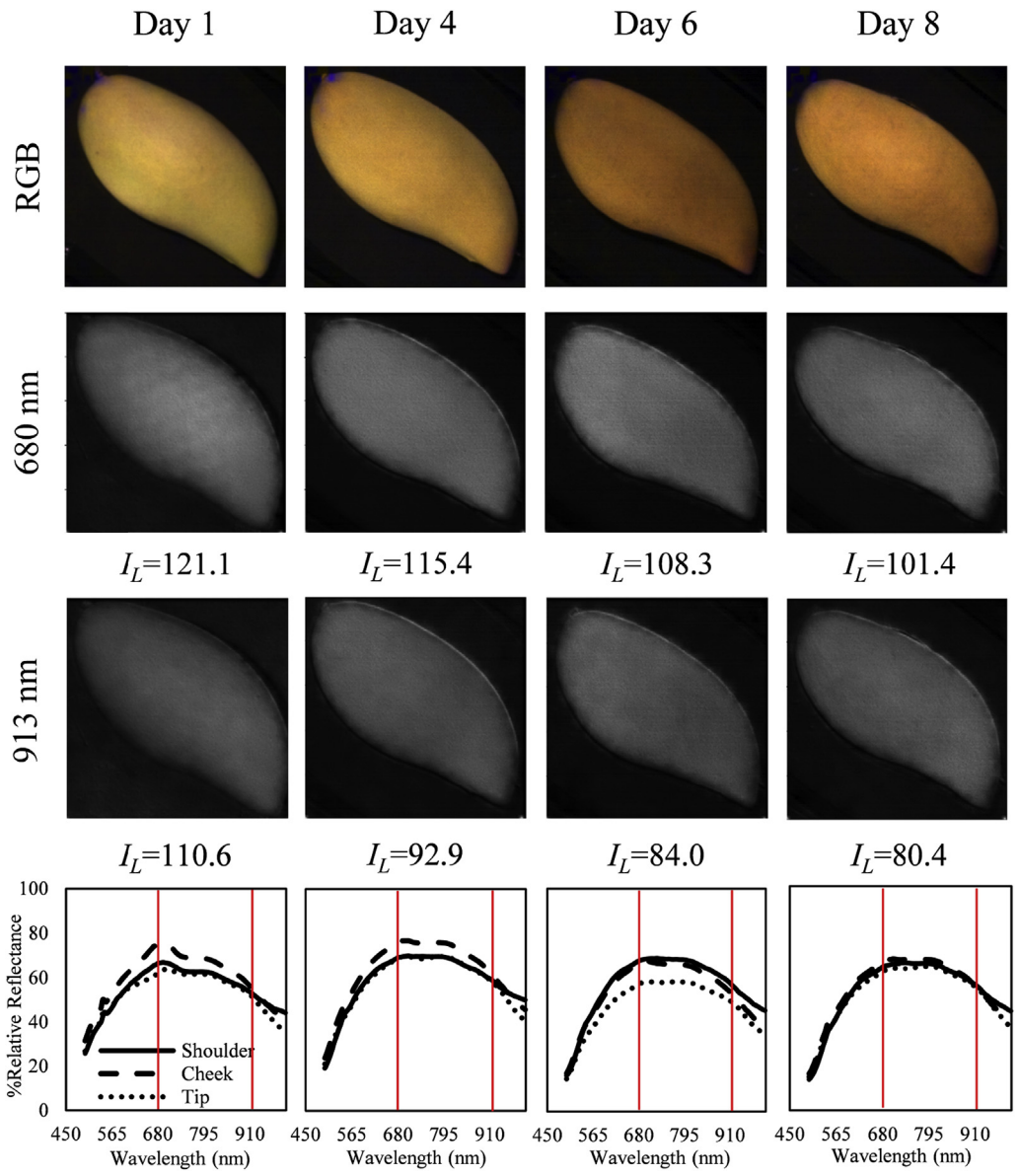

Fig. 4 – RGB images, monochromatic images at 680 and 913 nm and reflectance spectra at 1, 4, 6 and 8 days of ripening.

spectrum was acquired from the cheek section, while the lowest was found on tip section. The result corresponded with reference measurements, whereby the cheek part contained the lowest TSS content. In addition, correlations between I_L and physicochemical properties were examined. Significant correlations ($p < 0.05$) were found between I_L at 680 nm and TSS, TA and firmness with correlation coefficients (R) of −0.3, 0.53 and 0.68, respectively. Unexpected non-significant correlation was found between I_L at 913 nm and TSS ($p \geq 0.05$), while TA and firmness showed weak correlations with I_L with R of 0.34 and 0.57, respectively. Therefore, using the changes of I_L at these defined wavelengths was found to be inadequate for predicting the physicochemical properties of mango.

3.3. *Prediction models for physicochemical properties*

Table 1 shows the statistics of physicochemical properties in the calibration and validation sets for PLS analysis and regression results for mango qualities are summarised in Table 2. Scatter plots showing the predicted TSS, TA and firmness versus measured values are illustrated in Fig. 5. As shown in Table 2, prediction of fruit firmness by HSI was possible with R^2 of 0.77–0.81 and $RMSE_{val}$ of 2.83–3.15 N, and a slightly positive bias of 0.18–0.23 N. Calibration models for firmness developed from SG pre-processed spectra required a relatively higher number of PLS components to achieve comparable accuracy to other modelling techniques. Best prediction ability for firmness was found for the model from spectra pre-processed with MSC at R^2 of 0.81 and $RMSE_{val}$ of 2.85 N, with a bias of 0.20 N. TA was most accurately predicted by using the model developed from SNV spectra which gave R^2, $RMSE_{val}$, and a bias of 0.81, 0.24%, and −0.00%, respectively. Compared to firmness and TA, HSI showed less predictive ability for TSS attributes. The highest R^2 for TSS prediction model was found to be 0.5 with $RMSE_{val}$ of 2.0% and a bias of −0.0% using SNV pre-processed spectra with 13 PLS components (Table 2). The results showing pre-

Table 1 – Descriptive statistics of firmness, TA and TSS from reference analyses used for calibration and validation sets in PLS modelling.

	Calibration set (n = 108)[a]			Validation set (n = 52)		
	Mean	Range	SD	Mean	Range	SD
Firmness (N)	12.43	4.94–29.09	6.87	12.27	5.18–28.16	6.59
TA (%)	0.53	0.10–2.87	0.61	0.51	0.11–2.51	0.56
TSS (%)	18.0	8.8–25.6	3.1	18.0	11.0–22.8	2.8

[a] n = number of samples.

Table 2 – PLS components and accuracy of calibration and validation (RMSE & Bias) sets for firmness, TA and TSS using different pre-processing techniques for the data; bold treatments indicate best performance.

Quality attribute	Pre-processing[a]	PLS components	R^2	$RMSE_{cal}$	$RMSE_{val}$	Bias
Firmness (N)	None	15	0.79	2.68	3.01	0.18
	SG	37	0.79	2.78	3.00	0.16
	SG″	24	0.77	2.75	3.15	0.23
	SNV	18	0.81	2.52	2.83	0.22
	MSC	**14**	**0.81**	**2.54**	**2.85**	**0.20**
TA (%)	None	13	0.70	0.28	0.30	−0.00
	SG	36	0.69	0.28	0.31	−0.01
	SG″	23	0.73	0.29	0.29	−0.02
	SNV	**13**	**0.81**	**0.27**	**0.24**	**−0.00**
	MSC	14	0.79	0.27	0.25	0.00
TSS (%)	None	14	0.4	2.0	2.1	−0.0
	SG	21	0.4	2.0	2.1	0.0
	SG″	16	0.4	2.1	2.2	0.0
	SNV	**13**	**0.5**	**2.0**	**2.0**	**−0.0**
	MSC	12	0.5	2.0	2.1	0.0

[a] Savitzky–Golay smoothing (SG), Savitzky–Golay second derivative (SG″), standard normal variate transformation (SNV) and multiplicative scatter correction (MSC).

processing spectra with SNV technique gave the most accurate prediction model for mango quality attributes. MLR analysis showed 16 significant factors for firmness, 17 for TA, and 20 for TSS, with the top weighted coefficients at 510 and 574 nm for firmness, 506 and 530 nm for TA, and 506, 586, and 730 nm for TSS (Table 3). The results of MLR models were not substantially different in terms of prediction performance as compared to PLS. This would allow the elimination of unnecessary channels for prediction and would decrease time-consuming computations for quicker handling during industrial application.

3.4. *Spatial evaluation of physicochemical properties*

Results of HSI prediction maps for firmness, TA and TSS are shown in Fig. 6. The intensity of the individual qualities is indicated by a blue-red (in the web version) colour scale representing low to high values, respectively. Mean values from three positions of the reference measurements and predicted values from HSI (in brackets) are located below each sample. For firmness, fruit softening was observed from the distribution map with the shoulder part exhibiting intense blue colour which implies that firmness declined from the shoulder toward to tip part of the fruit. Similar results were found for a hybrid mango cultivar, which confirmed that ripening process occurred from stem to tip positions of the fruit (Jha, Sethi et al., 2010). However, the uniform softened texture as visualised by even blue colour was observed in fruits later during ripening. The variation of TA was consistent with laboratory reference values indicating that the tip sections in unripe fruits were more acidic than shoulder sections in riper fruits. The variations of TSS content in individual fruits were clearly seen in distribution maps. The intense red colour over the shoulder position compared with other positions represents the higher TSS regions. Nevertheless, uniform distribution of TSS was found in fully ripened fruits due to the complete conversion of starches to sugars (Medlicott & Thompson, 1985). Firmness was the parameter most accurately predicted by HSI. Meanwhile, the results for TSS were uncertain and the capacity of HSI to predict TA was mostly likely a secondary effect due to correlation with firmness.

Results for DA classification analysis for firmness are presented in Table 4. Samples were classified into three stages including unripe, ripe and overripe groups: fruits which had firmness value >14.0 N were grouped into unripe phase, while fruits having firmness value <8.0 N were classified as overripe and those with firmness value of 8.0–14.0 were defined as ripe phase. According to this classification, the major ripening stage of the fruit was ripe phase (60 fruits) followed by overripe (54 fruits) and unripe phase (46 fruits). Three-fourths of samples, consisting of all three ripening stages, were defined as the training set for development of the classification model and the remaining samples were used to validate the efficiency of classification. Overall, the DA was most successful at classifying unripe and overripe fruits, with ripe fruits being misclassified into either of the other two classes. Effective classification was realised in unripe fruits at values up to 89%.

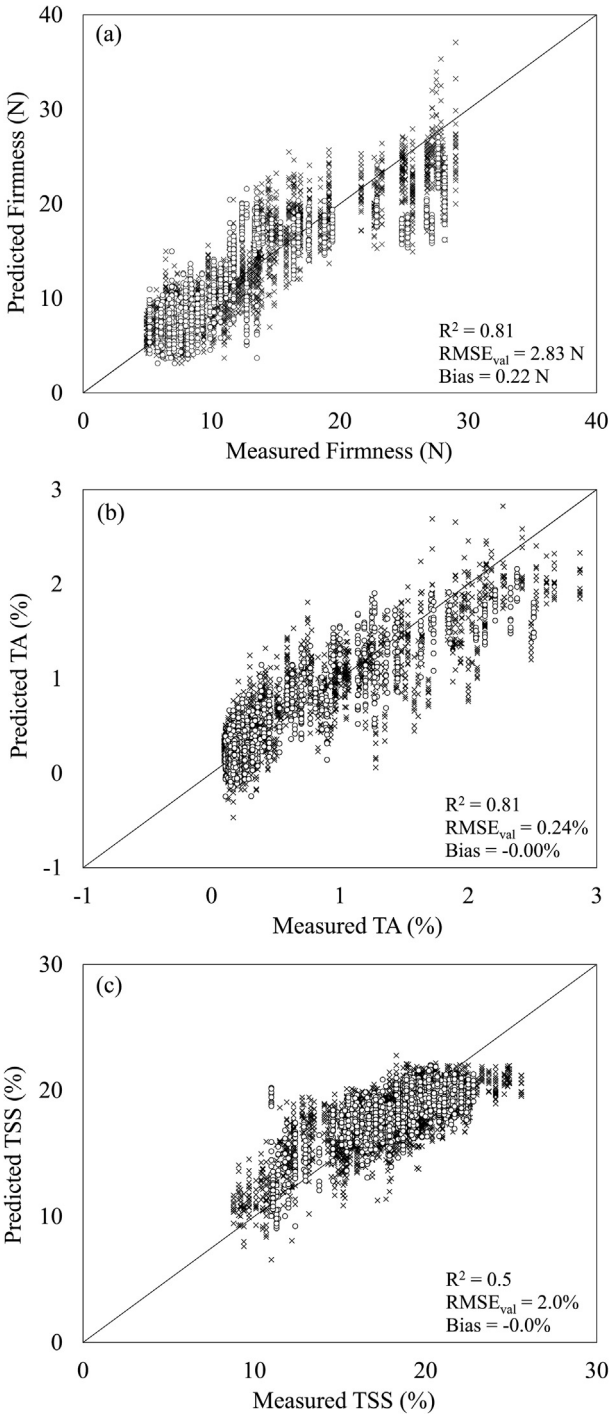

Fig. 5 – Prediction of (a) firmness, (b) TA and (c) TSS using SNV pre-processed spectra as compared to reference measurements; crossed and round symbols represent calibration and validation set, respectively.

4. Discussion

A spatial gradient of physicochemical parameters was observed for mango fruits showing non-uniform ripening process within individual samples. As reported by Crisosto, Slaughter, Garner, and Boyd (2001) and Peiris, Dull, Leffler, and Kays (1999), the ripening process and spatial distribution of the physicochemical constituents are dependent on fruit cultivar, production season, and fruit size. The pattern of TSS, higher in shoulder section then progressively decreasing toward the tip section, was also observed in mango cv. Hayden (Peiris et al., 1999). However, inconsistent results were found in mango cv. Cogshall showing mesocarp located in the tip part had significant higher TSS than the cheek and the shoulder of the fruit (Nordey, Joas, Léchaudel, Génard, & Joas, 2014). In this study, insignificant differences of TSS between shoulder and tip section could be explained by the variation of ethylene gradients in the mesocarp. Since a shorter distance exists between endocarp and pericarp at the shoulder, ethylene diffusion from the endocarp through the mesocarp and to the endocarp occurs quicker at the shoulder, thus causing faster ripening, e.g. higher TSS content (Nordey et al., 2014). From the results, changes of TA and TSS at each fruit position during ripening implied that ripening started from shoulder toward to tip part.

Changes caused by mango ripening can be roughly observed from mono-spectral (greyscale) images. These findings agreed with the other studies which explained that high firmness and low soluble solid content or unripe samples provided higher reflectance than ripe samples (ElMasry et al., 2007; Leiva-Valenzuela, Lu, & Aguilera, 2013; Rajkumar, Wang, ElMasry, Raghavan, & Gariepy, 2012; Wei, Liu, Qiu, Shao, & He, 2014). In this respect, SNV pre-processing exhibited the best prediction results since non-uniform scattering effects are reduced, i.e. baseline shifts and slope variations which are influenced by different physical property of fruit are minimised. Good prediction performance was achieved for firmness ($RMSE_{val}$ = 2.85 N, bias = 0.20 N) rather than for TA ($RMSE_{val}$ = 0.24%, bias = −0.00%) and TSS ($RMSE_{val}$ = 2.0%, bias = −0.0%). In other studies, firmness of persimmon could be related to HSI data with R^2 and RMSE of 0.83 and 4.35 N, respectively (Wei et al., 2014). Comparing the results with other mango cultivars, firmness prediction models developed in this study obtained higher R^2 and higher error (R^2 of 0.81 and RMSE of 2.83 N) than another model for Tommy Atkins (R^2 of 0.77 and SEP of 2.08 N) (Sivakumar, 2006). High RMSE found for the TA model greatly affected the accuracy as seen by the predicted negative values at low concentrations (Fig. 5b). However, the results from Baiano, Terracone, Peri, and Romaniello (2012) showed that HSI provided a higher accuracy for TA prediction in white grape and red grape with R^2 of 0.95 and 0.82 and RMSE of 0.06 and 0.24 g L^{-1}, respectively. Meanwhile, lower prediction ability was observed for TSS. Low R^2 (0.5) with high prediction error (2.0%) was stated as inadequate to use for screening quality of fruit.

Better performance of HSI for firmness and TA prediction rather than TSS prediction can be explained by the fact that HSI technique relies on scattering measurements which are more influenced by the structural features of the fruit tissue (Mendoza, Lu, Ariana, Cen, & Bailey, 2011). Moreover, the broader range of firmness and TA data as compared to TSS could have promoted stronger HSI correlations (Leiva-Valenzuela et al., 2014). The higher potential of HSI to predict firmness over TSS was also reported by Rajkumar et al. (2012) who found that HSI at 400–1000 nm showed a better prediction of firmness (R^2 = 0.91) than TSS (R^2 = 0.85) of banana.

Table 3 – Results of multiple linear regression (MLR) showing selected wavelengths and coefficients for firmness, TA and TSS.

Firmness		TA		TSS	
Wavelength	Coefficient	Wavelength	Coefficient	Wavelength	Coefficient
490	−14.93	490	−1.40	490	5.26
510	21.72	506	1.77	506	−13.51
514	13.25	510	1.41	522	5.34
538	−18.01	514	0.86	538	4.55
558	−3.90	530	−1.87	542	−4.28
562	−17.17	534	−1.32	546	2.69
574	21.95	538	−0.42	558	−5.45
602	−8.38	542	0.72	586	−12.72
618	7.48	546	−0.16	602	5.16
622	7.48	582	0.59	634	3.45
646	4.00	638	0.37	666	4.50
678	−8.63	670	−0.29	682	−3.40
710	5.35	682	−0.58	686	−2.10
758	−15.91	698	0.54	718	3.10
946	−6.31	706	0.25	730	−14.95
950	5.77	726	0.66	762	5.19
		754	−0.94	778	7.80
				794	−6.40
				954	−0.94
				994	−2.09

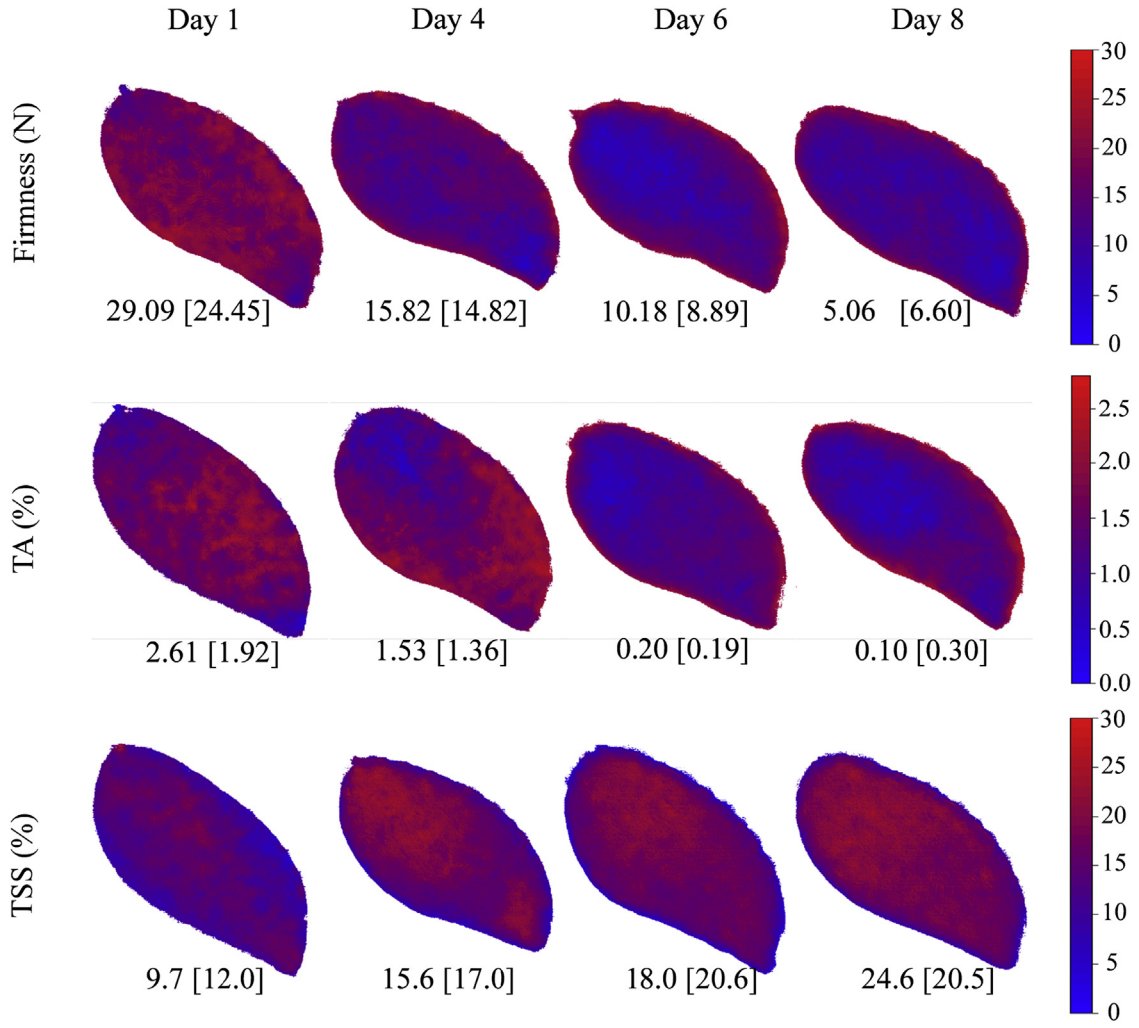

Fig. 6 – Prediction maps showing the distribution of firmness, TA and TSS in twelve mango samples during ripening with measured and predicted (in brackets) values indicating results of the HSI prediction model.

Table 4 – Results from discriminate analysis (DA) of firmness with classification performance according to ripeness groups: unripe (1), ripe (2) and overripe (3).

		Calibration (n[a] = 160)				Cross-validation (n = 120)			
		Predicted				Predicted			
		1	2	3	Total	1	2	3	Total
Measured									
n	1	41	5	0	46	26	8	0	34
	2	4	43	13	60	6	22	17	45
	3	0	6	48	54	0	4	37	41
%	1	89.1	10.9	0	100	76.5	23.5	0	100
	2	6.7	71.7	21.7	100	13.3	48.9	37.8	100
	3	0	11.1	88.9	100	0	9.8	90.2	100

[a] n = number of samples.

However, models established in this study could at least be used for rough screening due to excessive prediction error. The distribution of firmness within fruit was documented as an advantage of the HSI technique and analysis of the variation in hyperspectral maps is proposed as a possibility for grading systems in packing houses for quantitative and qualitative quality determination. Although considerable error was found for TA and TSS prediction models, the changes of these attributes within fruit during ripening were still possible to observe in prediction maps. False mapping occurred at the edge of the fruits resulting from the non-uniform distribution of light source on the curved fruit surface which caused stretching and shadowing (Gómez-Sanchis et al., 2008; Vélez Rivera et al., 2014). In this study, error from insufficient illumination was minimised by placing light diffusers near the fruit. The challenge of using diffusers to optimise light distribution for HSI was also reported for a study on mandarin by Gómez-Sanchis et al. (2008). Meanwhile, cross-polarisation of light could be a factor to further enhance the proficiency of HSI measurements (Nguyen-Do-Trong, Keresztes, De Ketelaere, & Saeys, 2016). Overall, applying additional methods for correcting the effect of the illumination system may enhance the spatial reliability of the prediction models.

The results of DA analysis for classification of fruit according to firmness as an indicator of ripeness were promising. Classification success rates greater than 90% are mostly desirable since losses of up to 10% in general are economically tolerable, but this level was not yet achieved. However, optimisation of the HSI measurements should improve the performance in order to allowing grading of unripe fruits according to maturity. The advantage of HSI technique to visualise differences in physicochemical parameters could enrich the characterisation of fruit ripening and develop sorting capabilities for industrial handling and processing of mango, especially in comparison to single point measurements. Overall, results and technology for detailing non-uniform ripening within individual fruits are beneficial for optimising postharvest aspects such as packing strategies and design, transport management, and marketing as well as preventing postharvest losses. The use of a hyperspectral frame "snapshot" camera with quick integration time for real-time measurements and the reduction of computing requirements via wavelength selection by MLR show good potential for use in fruit grading according to physicochemical properties. Indeed, the system exhibited short integration time, requiring only 10 ms for image acquisition. In comparison, "brush-broom" line-scanning HSI systems require around 2 s per fruit in the cases of apple and blueberry (Leiva-Valenzuela et al., 2014; Mendoza et al., 2011) and up to 80 s per fruit or 115 s per image in the cases of banana and grapes, respectively (Baiano et al., 2012; Rajkumar et al., 2012). With an additional processing time of about 85 ms (Yoon, Park, Lawrence, Windham, & Heitschmidt, 2011) per image required for HSI prediction using a programmed algorithm, this would equate to industrial throughput capacity of 3780 fruits, or approximately 1.32 t, per hour. Most interesting would be to realise strong classification ability for less ripened fruits, as this is the desirable stage to correctly identify at commercial packing houses.

5. Conclusion

The feasibility of using HSI techniques for mango quality assessment has been established in this study. The use of novel frame camera in the spectral region of 450–998 nm facilitated rapid image acquisition (10 ms per fruit) and the performance of prediction models for quality was not compromised after wavelength selection by MLR, which reduced the variables and computing requirements for HSI prediction models. The strongest relations were found for firmness followed by TA and TSS, however the results for the latter could be due to secondary correlations with firmness. The spatial distribution of firmness, TA and TSS content obtained from HSI-based prediction maps explained the robustness of PLS model and provided spatial information of ripening behaviour of mango. The ability of HSI for classifying fruit ripeness based on firmness was encouraging, although further improvement is needed conceivably via approaches such as increased population size and advanced subsampling methods, and improved measurement conditions. Based on the current results, HSI can already be considered as a potential technique for non-destructive grading of mango ripeness.

Acknowledgements

This study was conducted within the framework of SFB 564 project T4 funded by Deutsche Forschungsgemeinschaft (DFG), Germany. The Swift Co., Ltd., Thailand as well as staff at Silpakorn University are also gratefully acknowledged for their support. The authors would like to thank the Fiat Panis foundation for providing a scholarship. In addition, one of the authors (B.M.) would like to extend gratitude to the Food Security Center, University of Hohenheim and the DAAD (German Academic Exchange Service) for granting a visiting professor fellowship. The authors wish to dedicate this work in commemoration of Mr. Paichayon Uathaveekul.

REFERENCES

AOAC. (1999). *Acidity (titratable) of fruit products. (AOAC method 942.15)* (16th ed.). Gaithersburg, MD: Association of Official Analytical Chemists. Official Methods of Analysis.

Baiano, A., Terracone, C., Peri, G., & Romaniello, R. (2012). Application of hyperspectral imaging for prediction of physico-chemical and sensory characteristics of table grapes. *Computers and Electronics in Agriculture, 87*, 142–151.

Beleites, C., & Sergo, V. (2012). *HyperSpec: A package to handle hyperspectral data sets in R*. R package version 0.98–20120923 http://hyperspec.r-forge.r-project.org/index.html.

Crisosto, C. H., Slaughter, D. C., Garner, D., & Boyd, J. (2001). Stone fruits critical bruising thresholds. *Journal American Pomological Society, 55*(2), 76–81.

Delwiche, S. R., Mekwatanakarn, W., & Wand, C. Y. (2008). Soluble solids and simple sugars measurement in intact mango using near infrared spectroscopy. *HortTechnology, 18*, 410–416.

ElMasry, G. M., & Nakauchi, S. (2016). Image analysis operations applied to hyperspectral images for non-invasive sensing of food quality – A comprehensive review. *Biosystems Engineering, 142*, 53–82.

ElMasry, G., Sun, D., & Allen, P. (2013). Chemical-free assessment and mapping of major constituents in beef using hyperspectral imaging. *Journal of Food Engineering, 117*(2), 235–246.

ElMasry, G., Wang, N., ElSayed, A., & Ngadi, M. (2007). Hyperspectral imaging for nondestructive determination of some quality attributes for strawberry. *Journal of Food Engineering, 81*(1), 98–107.

Esbensen, K. H. (2004). *Multivariate data analysis-in practice* (5th ed.). Norway: CAMO Process AS.

Gómez-Sanchis, J., Moltó, E., Campls-Valls, G., Gómez-Chova, L., Aleixos, N., & Blasco, J. (2008). Automatic correction of the effects of the light source on spherical objects. An application to the analysis of hyperspectral images of citrus fruits. *Journal of Food Engineering, 85*, 191–200.

Haff, R. P., Saranwong, S., Thanapase, W., Janhiran, A., Kasemsumran, S., & Kawano, S. (2013). Automatic image analysis and spot classification for detection of fruit fly infestation in hyperspectral images of mangoes. *Postharvest Biology and Technology, 86*, 23–28.

Hagen, N., Kester, R. T., Gao, L., & Tkaczyk, T. S. (2012). Snapshot advantage: A review of the light collection improvement for parallel high-dimensional measurement systems. *Optical Engineering, 51*(11), 111702–111711.

Jha, S. N., Kingsly, A. R. P., & Chopra, S. (2006). Physical and mechanical properties of mango during growth and storage for determination of maturity. *Journal of Food Engineering, 72*(1), 73–76.

Jha, S. N., Narsaiah, K., Sharma, A. D., Sing,h, M., Bansal, S., & Kumar, R. (2010). Quality parameters of mango and potential of non-destructive techniques for their measurement - A review. *Journal of Food Science and Technology, 47*(1), 1–14.

Jha, S. K., Sethi, S., Srivastav, M., Dubey, A. K., Sharma, R. R., Samuel, D. V. K., et al. (2010). Firmness characteristics of mango hybrids under ambient storage. *Journal of Food Engineering, 97*(2), 208–212.

Jung, A., Vohland, M., & Thiele-Bruhn, S. (2015). Use of a portable camera for proximal soil sensing with hyperspectral image data. *Remote Sensing, 7*(9), 11434–11448.

Ketsa, S., Chidtragool, S., Klein, J. D., & Lurie, S. (1998). Effect of heat treatment on changes in softening, pectic substances and activities of polygalacturonase, pectinesterase and β-galactosidase of ripening mango. *Journal of Plant Physiology, 153*, 457–461.

Kienzle, S., Sruamsiri, P., Carle, R., Sirisakulwat, S., Spreer, W., & Neidhart, S. (2012). Harvest maturity detection for 'Nam Dokmai #4' mango fruit (*Mangifera indica* L.) in consideration of long supply chains. *Postharvest Biology and Technology, 72*, 64–75.

Leiva-Valenzuela, G. A., Lu, R., & Aguilera, J. M. (2013). Prediction of firmness and soluble solids content of blueberries using hyperspectral reflectance imaging. *Journal of Food Engineering, 115*(1), 91–98.

Leiva-Valenzuela, G. A., Lu, R., & Aguilera, J. M. (2014). Assessment of internal quality of blueberries using hyperspectral transmittance and reflectance images with whole spectra or selected wavelengths. *Innovative Food Science & Emerging Technologies, 24*, 2–13.

Magwaza, L., & Opara, U. (2015). Analytical methods for determination of sugars and sweetness of horticultural products - A review. *Scientia Horticulturae, 184*, 179–192.

Makino, Y., Isami, A., Suhara, T., Oshita, S., Tsukada, M., Ishiyama, R., et al. (2013). Non-destructive analysis of internal and external qualities of mango fruits during storage by hyperspectral imaging. *Acta Horticulturae, 1011*, 443–450.

McGlone, V. A., & Kawano, S. (1998). Firmness, dry-matter and soluble-solids assessment of postharvest kiwifruit by NIR spectroscopy. *Postharvest Biology and Technology, 13*(2), 131–141.

Medlicott, A. P., & Thompson, A. K. (1985). Analysis of sugars and organic acids in ripening mango fruit (*Mangifera indica* L. var. Keitt) by high performance liquid chromatography. *Journal of the Science of Food and Agriculture, 36*, 561–566.

Mendoza, F., Lu, R., Ariana, D., Cen, H., & Bailey, B. (2011). Integrated spectral and image analysis of hyperspectral scattering data for prediction of apple fruit firmness and soluble solids content. *Postharvest Biology and Technology, 62*(2), 149–160.

Mevik, B.-H., & Wehrens, R. (2007). The PLS package: Principal component and partial least squares regression in R. *Journal of Statistical Software, 18*(2), 1–24.

Nagle, M., Mahayothee, B., Rungpichayapichet, P., Janjai, S., & Müller, J. (2010). Effect of irrigation on near-infrared (NIR) based prediction of mango maturity. *Scientia Horticulturae, 125*(4), 771–774.

Nguyen-Do-Trong, N., Keresztes, J. C., De Ketelaere, B., & Saeys, W. (2016). Cross-polarised VNIR hyperspectral reflectance imaging system for agrifood products. *Biosystems Engineering, 151*, 152–157.

Nordey, T., Joas, J., Léchaudel, M., Génard, M., & Joas, J. (2014). Spatial and temporal variations in mango colour, acidity, and sweetness in relation to temperature and ethylene gradients within the fruit. *Journal of Plant Physiology, 171*, 1555–1563.

Palafox-Carlos, H., Yahia, E., Islas-Osuna, M. A., Gutierrez-Martinez, P., Robles-Sánchez, M., & González-Aguilar, G. A. (2012). Effect of ripeness stage of mango fruit (*Mangifera indica* L. cv. Ataulfo) on physiological parameters and antioxidant activity. *Scientia Horticulturae, 135*, 7–13.

Peiris, K. H. S., Dull, G. G., Leffler, R. G., & Kays, S. J. (1999). Spatial variability of soluble solids or dry-matter content within individual fruits, bulbs, or tubers: Implications for the development and use of NIR spectrometric techniques. *HortScience, 34*(1), 114–118.

Pu, Y. Y., & Sun, D. W. (2015). Vis-NIR hyperspectral imaging in visualizing moisture distribution of mango slices during microwave-vacuum drying. *Food Chemistry, 188*, 271–278.

R Core Team. (2014). *R: A language and environment for statistical computing*. Vienna, Austria: R Foundation for Statistical Computing. https://www.R-project.org.

Rajkumar, P., Wang, N., ElMasry, G., Raghavan, G. S. V., & Gariepy, Y. (2012). Studies on banana fruit quality and

maturity stages using hyperspectral imaging. *Journal of Food Engineering, 108*(1), 194–200.
Rasband, W. S. (2014). *ImageJ, U. S.* Bethesda, Maryland, USA: National Institutes of Health. http://imagej.nih.gov/ij/.
Rungpichayapichet, P., Mahayothee, B., Khuwijitjaru, P., Nagle, M., & Müller, J. (2015). Non-destructive determination of β-carotene content in mango by near-infrared spectroscopy compared with colorimetric measurements. *Journal of Food Composition and Analysis, 38*, 32–41.
Rungpichayapichet, P., Mahayothee, B., Nagle, M., Khuwijitjaru, P., & Müller, J. (2016). Robust NIRS models for non-destructive prediction of postharvest fruit ripeness and quality in mango. *Postharvest Biology and Technology, 111*, 31–40.
Saranwong, S., Haff, R. P., Thanapase, W., Janhiran, A., Kasemsumran, S., & Kawano, S. (2011). A feasibility study using simplified near infrared imaging to detect fruit fly larvae in intact fruit. *Journal of Near Infrared Spectroscopy, 19*, 55–60.
Savitzky, A., & Golay, M. J. E. (1964). Smoothing and differentiation of data by simplified least squares procedures. *Analytical Chemistry, 36*(8), 1627–1639.
Schmilovitch, Z., Ignat, T., Alchanatis, V., Gatker, J., Ostrovsky, V., & Felföldi, J. (2014). Hyperspectral imaging of intact bell peppers. *Biosystems Engineering, 117*, 83–93.
Sivakumar, S. S. (2006). *Potential applications of hyperspectral imaging for the determination of total soluble solids, water content and firmness in mango*. Master thesis. Canada: McGill University.
Sivakumar, D., Jiang, Y., & Yahia, E. M. (2011). Maintaining mango (*Mangifera indica* L.) fruit quality during the export chain. *Food Research International, 44*, 1254–1263.
Stevens, A., & Ramirez-Lopez, L. (2013). An introduction to the prospectr package. R package Vignette R package version 0.1.3. ftp://200.236.31.2/CRAN/web/packages/prospectr/vignettes/prospectr-intro.pdf
Subedi, P. P., & Walsh, K. B. (2011). Assessment of sugar and starch in intact banana and mango fruit by SWNIR spectroscopy. *Postharvest Biology and Technology, 62*(3), 238–245.
Theanjumpol, P., Self, G., Rittiton, R., Pankasemsuk, T., & Sardsud, V. (2014). Quality control of mango fruit during postharvest by near infrared spectroscopy. *Chiang Mai University Journal of Natural Sciences, 13*(2), 141–157.
Valente, M., Leardi, R., Self, G., Luciano, G., & Pain, J. P. (2009). Multivariate calibration of mango firmness using vis/NIR spectroscopy and acoustic impulse method. *Journal of Food Engineering, 94*(1), 7–13.
Vélez Rivera, N., Blasco, N., Chanona-Pérez, J., Calderón-Domínguez, G., de JesúsPerea-Flores, M., Arzate-Vázquez, I., et al. (2014). Computer vision system applied to classification of "Manila" mangoes during ripening process. *Food and Bioprocess Technology, 4*, 1183–1194.
Watanawan, C., Wasusri, T., Srilaong, V., Wongs-Aree, C., & Kanlayanarat, S. (2014). Near infrared spectroscopic evaluation of fruit maturity and quality of export Thai mango (*Mangifera indica* L. var. Namdokmai). *International Food Research Journal., 21*(3), 1109–1114.
Wei, X., Liu, F., Qiu, Z., Shao, Y., & He, Y. (2014). Ripeness classification of astringent persimmon using hyperspectral imaging technique. *Food and Bioprocess Technology, 7*(5), 1371–1380.
Yashoda, H. M., Prabha, T. N., & Tharanathan, R. N. (2006). Mango ripening: Changes in cell wall constituents in relation to textural softening. *Journal of the Science of Food and Agriculture, 86*(5), 713–721.
Yoon, S. C., Park, B., Lawrence, K. C., Windham, W. R., & Heitschmidt, G. W. (2011). Line-scan hyperspectral imaging system for real-time inspection of poultry carcasses with fecal material and ingesta. *Computers and Electronics in Agriculture, 79*(2), 159–168.
Zhang, X., Liu, F., He, Y., & Gong, X. (2013). Detecting macronutrients content and distribution in oilseed rape leaves based on hyperspectral imaging. *Biosystems Engineering, 115*, 56–65.